Multifaceted Transient Stability Analysis of Power Systems: A Study of Synchronizing Torque in Conventional Systems and Energy Functions in Renewable Connected Systems

PhD Defense

Albert Poulose (PhD Candidate) Soobae Kim (Professor)

Department of Electrical Engineering
School of Electronic and Electrical Engineering
Kyungpook National University, Daegu 41566, South Korea

November 29, 2024

Overview

1. Background & Problem Statement
2. Synchronizing Torque-based TSA of Conventional Power System
3. Energy Function-based TSA of Renewable Connected Power System
4. Conclusion
5. Supplementary Informations

*TSA = Transient Stability Analysis

Overview

IEEE Classification of Power System Stability 2020

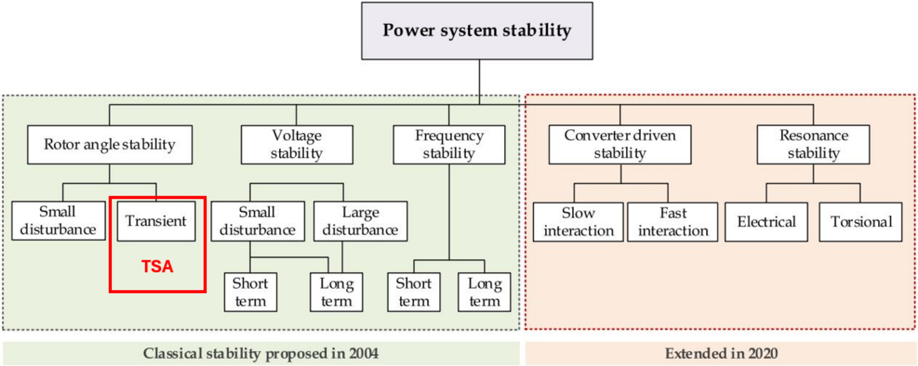

Figure 1: Power System Stability Classification.

1

[1] Hatziargyriou, Nikos, et al. "Definition and classification of power system stability–revisited & extended." IEEE Transactions on Power Systems 36.4 (2020): 3271-3281.

Transient Stability Analysis (TSA)

Transient Stability

- Is the ability of the power system to maintain synchronism when subjected to a severe transient disturbance.
- Resulting system response involves large excursions of generator rotor angles and is influenced by the nonlinear power-angle relationship.
- Stability depends on both the initial operating state of the system and the severity of the disturbance.

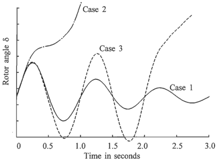

Figure 2: Rotor angle response to a transient disturbance.

- **Case 1:** Rotor angle increases to a maximum, then decreases and oscillates with decreasing amplitude until it reaches a steady state (stable case).
- **Case 2:** Rotor angle continues to increase steadily until synchronism is lost (first-swing instability).
- **Case 3:** System is stable in its first swing but becomes unstable due to growing oscillations as the end state approaches.

NOTE

Study period of interest is usually limited to **3 to 5 seconds** following the disturbance, although it **may extend to about 10 seconds** for very large systems with dominant interarea modes of oscillations.

2

[2] Kundur, Prabha. "Power system stability." Power system stability and control 10 (2007): 7-1.

Why TSA is important?

- Prevention of System collapse (Blackouts): Avoidance of cascading failures
- Protection of Equipment: Avoiding mechanical stress and prolonging the lifespan of the equipment
- Integration of Renewable Energy Sources: Managing expansions in existing power systems
- Facilitating Load Changes and Growth: Handling sudden load changes in the system ensures that the system can adapt to these changes without losing synchronism
- Optimization of System Performance: Enabling engineers to pinpoint areas prone to instability
- Ensuring Reliability of Power Supply: Sustained operation of power supply
- Economic Implications: Avoiding economic losses associated with power interruptions
- Support for System Protection Schemes: Coordination with protection systems
- Maintenance of Power Quality: Minimizing voltage fluctuations

Different TSA Methodologies

Non-Lyapunov Based Methods

1. Synchronizing Torque based analysis:⇒ Simplified calculations based on linearized models.
   - Evaluate the synchronizing torque coefficient, which relates to how effectively the system can restore generator angles back to synchronism after a disturbance.
2. Time-domain (t-d) simulation ⇒ Get time responses of state variables.
   - Numerical integration methods: Eulers, RK and Trapezoidal methods.
   - Require high computation and more time for solving non-linear differential-algebraic equations due to the bulk power systems' large dimensionality and nonlinearity.
3. Graphical Methods:
   - Frequency versus angle plots ⇒ Phase portrait plots
   - Power, frequency, voltage versus angle plots ⇒ Concept of Equal area criterion (EAC) is utilized.
4. Data-driven based methods ⇒ Machine learning and artificial intelligence based methods

Lyapunov(2nd) Based Methods (Direct TSA Methods)

1. Energy function method ⇒ Most mature and applicable for both *SMIB* and multi-machine systems
2. Sum-of-squares based method ⇒ Proposed in the last decade and systematically constructed Lyapunov functions for complex power systems.
3. Other Lyapunove-based methods ⇒ Decentralized stability analysis methods, Lur'e type Lyapunov functions, Hamilton functions, and Extended Lyapunov functions-based methods.

3

[3] Wu, Qing-Hua, et al. "Transient stability analysis of large-scale power systems: A survey." CSEE Journal of Power and Energy Systems 9.4 (2023).

Objective 1: TSA of Conventional Power System

Research Gap

- Traditionally, *TSA* through synchronizing torque values of each generator is determined based on the total synchronizing torque contributions from the generator to the network through the system approximations.
- This *TSA* indicate individual generators' approximate transient stability margin without considering other connected generator synchronizing torque interactions accurately.

Objective

A model-based *TSA* index for each generator is proposed from the synchronizing torque contributions of all other connected generators in a multi-machine interconnected power system.

- It is a new interpretation of the generator's synchronizing torque in terms of electromechanical oscillation modes to consider the synchronizing torque interactions among generators.
- The popular *TSA* indicator **critical clearing time (CCT)** and the **traditionally determined *TSA* through synchronizing torque** need to be calculated to verify and compare the performance of the proposed transient stability index.

Renewable connected power system

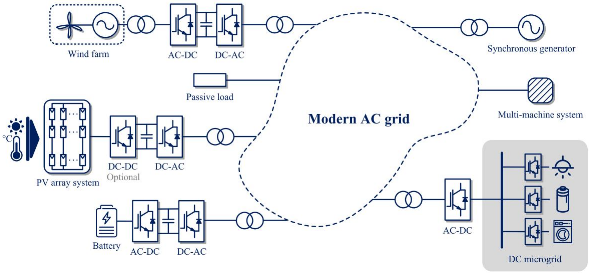

Figure 3: Modern AC grid.

NOTE

The inverters in renewable connected power systems **decouple electromechanical oscillations or disturbances from the grid**; hence, the proposed *TSA* index in objective 1 cannot be directly used in modern grids with renewable sources.

[4]

[4] Peng, Qiao, et al. "On the stability of power electronics-dominated systems: Challenges and potential solutions." IEEE Transactions on Industry Applications 55.6 (2019): 7657-7670.

TSA studies in Renewable connected power systems

Classifications

1. Studies involving single voltage source converters (*VSC*) connected to the grid.
   - The most recent research in single *VSC*s tends to concentrate on power electronic notions and often uses traditional *TSA* approaches, together with *EMT*-based *t-d* simulations and hardware-based investigations.
2. Studies with multiple *VSC* connected to the grid.
   - There is a relative paucity of research on grid-connected systems incorporating grid-forming VSCs (*GFM-VSC*) compared to studies involving multiple grid-following VSCs (*GFL-VSC*).

Multiple *VSC* reveal three sub-categories:

1. *TSA* studies focusing solely on *GFL-VSC*
2. Those concentrating exclusively on *GFM-VSC*
3. Those examining systems with both *GFL* and *GFM* *VSC* interconnected to the grid.

Research Gap

- Despite the increasing preference for *GFM-VSC*s over the past decade due to their inherent benefits to transient stability, the literature predominantly features single *GFM-VSC* grid-connected studies employing various *TSA* approaches.
- However, studies examining systems that combine *GFL-VSC* and *GFM-VSC* or involve multiple *GFM-VSC* grid connections remain limited. This gap highlights the need for researchers to devote more attention to this field.

Objective 2: TSA of Renewable Connected Power System

Objective

Proposes an innovative fast direct transient stability analysis (*DTSA*) approach that leverages Lyapunov's direct method to assess the transient stability of a *GFM-VSC* with a virtual synchronous machine (*VSM*) control technique, incorporating the influence of parallel-connected *GFL-VSC* control strategy.

- The proposed *DTSA* approach models the *GFL-VSC* as a current source with parallel internal reactance and the *GFM-VSC* as a voltage source with series internal reactance.
- Detailed analytical derivations of the *DTSA* approach using transient energy functions, along with the *DTSA* criterion for the interconnected system, need to be presented to determine the *CCT* of the *GFM-VSC*.
- Furthermore, electromagnetic transient (*EMT*) time-domain (t-d) simulation responses are needed to be utilized to validate the accuracy and computational effectiveness of the proposed fast *DTSA* approach.

Overview

Related Journal Publication

- Poulose, Albert, and Soobae Kim. "Synchronizing Torque-Based Transient Stability Index of a Multimachine Interconnected Power System." *Energies* 15.9 (2022): 3432.

Synchronizing Torque and TSA

- The synchronizing torque is an electrical torque component produced by interacting stator windings and a fundamental air-gap flux component of the synchronous generator (SG).
- During disturbances, the SG' magnetic fields' accumulated energy ensures precise immediate power support, and these magnetic fields are distributed according to the synchronizing torque coefficients (STC) of the multimachine interconnected power system.

Swing Equation of SMIB system

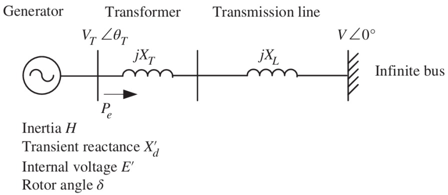

Figure 4: SMIB System.

- Describes the rotational motion of an SG's rotor in response to power imbalances.

$$\Delta\dot{\delta} = \Omega\Delta\omega \tag{1}$$

$$\begin{aligned} 2H\Delta\dot{\omega} &= T_m - T_e - D\Delta\omega \\ &= T_m - P_e - D\Delta\omega \\ &= T_m - \frac{E' V \sin\delta}{X_{eq}} - D\Delta\omega \end{aligned} \tag{2}$$

where δ (in radians) is the generator rotor angle with respect to the infinite bus, $\Delta\omega$ (in p.u.) is the machine speed deviation, $\Omega = 2\pi f$ is the conversion factor from p.u. speed to radians, and $X_{eq} = X_d' + X_T + X_L$.

- **Note**: power P is equal to the product of the torque T and the machine speed ω, that is, $P = T \cdot \omega$. However, with $\omega \approx 1$ pu even in transient conditions, it is possible to use the approximation $T \approx P$.

[5]

[5] Chow, Joe H., and Juan J. Sanchez-Gasca. Power system modeling, computation, and control. John Wiley & Sons, 2020.

Synchronizing Torque and TSA

In steady state

Equilibrium satisfies:

$$\Delta\omega = 0, \quad \frac{E' V \sin \delta_{ep}}{X_{eq}} = P_e = T_m \tag{3}$$

Linearization of Equations (1) and (2) at the equilibrium $\delta = \delta_{ep}$ and $\Delta\omega = 0$ results in:

$$\begin{aligned} \Delta\dot{\delta} &= \Omega\Delta\omega \\ 2H\Delta\dot{\omega} &= -\frac{\partial}{\partial\delta}\left(\frac{E' V \sin \delta}{X_{eq}}\right)\Big|_o \Delta\delta \\ &\quad - \frac{\partial}{\partial\Delta\omega}\left(D\Delta\omega\right)|_o\Delta\omega + \frac{\partial}{\partial\Delta\left(T_m\right)}|_o\Delta T_m \\ &= -K_s\Delta\delta - D\Delta\omega + \Delta T_m \end{aligned} \tag{4}$$

where

$$K_s = \frac{E' V \cos \delta_{ep}}{X_{eq}}$$

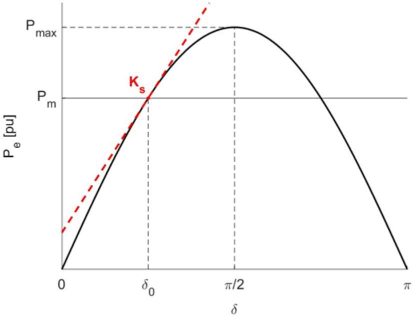

Figure 5: Power-Angle Curve.

- K_s is the *STC* signifies the ability of the generator to stay synchronized to the infinite bus.
- K_s will oppose $\Delta\delta$, and it should be a positive value to maintain the stability of the *SG*.

Linearized Models of Multimachine Power System

For a multimachine power system with N_G machines without considering damping torques, the swing equation of the i^{th} machine is defined as follows:

$$\Delta\dot{\delta}_i = \Omega\Delta\omega_i \tag{5}$$

$$\Delta\dot{\omega}_i = \frac{1}{2H_i}\left(\Delta P_{mi} - K_{sii}\Delta\delta_i + \sum_{j=1, j\neq i}^{N_G} K_{sij}\Delta\delta_j\right) \tag{6}$$

Since P_{mi} = constant and $2H_i^{-1} = M_i^{-1}$, Equation (6) can be rearranged as follows:

$$\Delta\dot{\omega}_i = M_i^{-1}\left(-K_{sii}\Delta\delta_i + \sum_{j=1, j\neq i}^{N_G} K_{sij}\Delta\delta_j\right) \tag{7}$$

for $i = 1, 2, ..., N_G$
[6] [7]

[6] Chow, Joe H., and Juan J. Sanchez-Gasca. Power system modeling, computation, and control. John Wiley & Sons, 2020.

[7] Sauer, Peter W., Mangalore A. Pai, and Joe H. Chow. Power system dynamics and stability: with synchrophasor measurement and power system toolbox. John Wiley & Sons, 2017.

Linearized Models of Multimachine Power System

where

δ_i i^{th} machine rotor angle

δ_j adjacent machine rotor angle

ω_i i^{th} machine rotor speed in pu

P_{mi} i^{th} machine mechanical power input

H_i i^{th} machine inertia constant

Ω $= 2\pi f$ is the per unit to radian conversion factor for the speed change.

K_{sii} $= \sum_{j=1, j\neq 1}^{N_G} E_i E_j \left(B_{ij} \cos\left(\delta_i - \delta_j\right)\right) - G_{ij} \sin\left(\delta_i - \delta_j\right)|_\circ$ are diagonal elements representing the total contribution of synchronizing torque from a machine to the network.

K_{sij} $= E_i E_j \left(B_{ij} \cos\left(\delta_i - \delta_j\right)\right) - G_{ij} \sin\left(\delta_i - \delta_j\right)|_\circ$ are off-diagonal elements representing the synchronizing torque interactions between the machines.

E_i $=$ constant voltage behind transient reactance of the machine i

Y_{ii} $= G_{ii} + jB_{ii}$ diagonal element of the network's short-circuit admittance matrix Y

Y_{ij} $= G_{ij} + jB_{ij}$ off-diagonal element of the network's short-circuit admittance matrix Y

Linearized Models of Multimachine Power System

The linearized multimachine power system's state-space form can be represented as follows using Equations (5) and (7)

$$\begin{bmatrix} \Delta\dot{\delta}_i \\ \Delta\dot{\omega}_i \end{bmatrix} = A \begin{bmatrix} \Delta\delta_i \\ \Delta\omega_i \end{bmatrix} \tag{8}$$

where

$$\text{A} = \begin{bmatrix} 0 & \Omega I \\ M_i^{-1} K_s & 0 \end{bmatrix}$$ is the system matrix,

$$M_i^{-1} = \begin{bmatrix} {M_1}^{-1} & \cdots & 0 \\ \vdots & \ddots & \vdots \\ 0 & \cdots & {M_{N_G}}^{-1} \end{bmatrix}$$ is the inertia constants of all *SM*s in diagonal matrix form.

$$K_s = \begin{bmatrix} -K_{s11} & \cdots & K_{s1N_G} \\ \vdots & \ddots & \vdots \\ K_{sN_G1} & \cdots & -K_{sN_GN_G} \end{bmatrix}$$ is the synchronizing torque coefficient (STC) matrix

REMARKS

- The traditional *TSA* method based on synchronizing torque utilizes the diagonal elements of the *STC* matrix to get each generator's approximate transient stability information.

Proposed Stability Index : Derivation & Explanations

In linearized power system models

The time-domain response of states can be expressed as the summation of n modes, as shown in Equation (9).

$$\Delta x(t) = \sum_{h=1}^{n} \left(w_h^T \Delta x_0 \right) v_h e^{\lambda_h t} \tag{9}$$

- The term $w_h^T \Delta x_0$ with a contribution factor of left eigenvector w_h represents the contribution of the initial state Δx_0 in the h^{th} mode.
- The right eigenvector represented by v_h denotes the mode shape and provides the participation of states in each mode, and λ_h is the h^{th} eigenvalue.

Using Equation (9), the i^{th} machine's rotor angle dynamic state variable can be represented in terms of eigenvectors for all n modes as shown in Equation (10).

$$\begin{aligned}
\Delta\delta_i(t) &= \sum_{h=1}^{n} \left(w_h^T \Delta\delta_{0i} \right) v_h e^{\lambda_h t} \\
&= w_1^T \Delta\delta_{0i} v_1 e^{\lambda_1 t} + w_2^T \Delta\delta_{0i} v_2 e^{\lambda_2 t} + \ldots + w_n^T \Delta\delta_{0i} v_n e^{\lambda_n t} \\
&= \Delta\delta_i^1(t) + \Delta\delta_i^2(t) + \ldots. + \Delta\delta_i^n(t) = \sum_{h=1}^{n} \Delta{\delta_i}^h(t)
\end{aligned} \tag{10}$$

where $\Delta\delta_{0i}$ indicates the i^{th} machines's initial rotor angle state variable, and the variable $\Delta\delta_i^h(t)$ represents the i^{th} machine's rotor angle change for the h^{th} mode.

Proposed Stability Index : Derivation & Explanations

Similarly,

$$\dot{\Delta\omega}_i(t) = \dot{\Delta\omega}_i^1(t) + \dot{\Delta\omega}_i^2(t) + ... + \dot{\Delta\omega}_i^n(t) = \sum_{h=1}^{n} \dot{\Delta\omega}_i^h(t) \tag{11}$$

Therefore, i^{th} machine's rotor speed change for the h^{th} mode can be formulated from Equation (7) as follows:

$$\dot{\Delta\omega}_i^h(t) = M_i^{-1}\left(-K_{sii}\Delta\delta_i{}^h(t) + \sum_{j=1,j\neq i}^{N_G} K_{sij}\Delta\delta_j{}^h(t)\right) \tag{12}$$

Proposed Index

The corresponding i^{th} machine's transient stability margin in terms of synchronizing torques, which includes the synchronizing torque contributions of the j^{th} machine's interactions for the h^{th} mode, is accurately formulated in Equation (13).

$$\frac{\dot{\Delta\omega}_i^h(t)}{\Delta\delta_i{}^h(t)} = M_i^{-1}\left(-K_{sii} + \frac{\sum_{j=1,j\neq i}^{N_G} K_{sij}\Delta\delta_j{}^h(t)}{\Delta\delta_i{}^h(t)}\right) \tag{13}$$

Remarks

- The synchronizing torque contributions from j^{th} generator on the i^{th} generator can be accommodated by the eigenvector (mode shape) relationship between the rotor angle dynamic states of the generators.
- However, the traditional *TSA* through *STC* does not consider the synchronizing torque interaction from other generators (*SMIB* approximations).

Proposed Stability Index: An Example Case

Note

- The proposed transient stability index is explained on a three-machine interconnected power system ($N_G = 3$) with negligible damping torques.
- For an interconnected power system holding N_G machines, there would be a $N_G - 1$ set of electromechanical oscillation modes generated from swing equations, and the fundamental behavior of these modes is solely caught in the rotor angle and speed dynamic variables.
  - Hence, there are two electromechanical oscillation modes ($n = 2$) for the generalized three-machine example system case.

From Equation (10), the three machines' rotor angle dynamic state's time response can be independently split in terms of the rotor angle dynamic state variables of two modes:

$$
\begin{aligned}
\Delta\delta_1(t) &= \Delta{\delta_1}^1(t) + \Delta{\delta_1}^2(t) \\
\Delta\delta_2(t) &= \Delta{\delta_2}^1(t) + \Delta{\delta_2}^2(t) \\
\Delta\delta_3(t) &= \Delta{\delta_3}^1(t) + \Delta{\delta_3}^2(t)
\end{aligned}
\tag{14}
$$

Equation (14) can be used to determine the other generator's synchronizing torque contribution factor for each mode separately.

Proposed Stability Index: An Example Case

For mode 1:

$$\begin{aligned}
\frac{\Delta\dot{\omega}_1^1(t)}{\Delta\delta_1{}^1(t)} &= M_1{}^{-1}\left(-K_{s11} + K_{s12}\frac{\Delta\delta_2{}^1(t)}{\Delta\delta_1{}^1(t)} + K_{s13}\frac{\Delta\delta_3{}^1(t)}{\Delta\delta_1{}^1(t)}\right) \\
\frac{\Delta\dot{\omega}_2^1(t)}{\Delta\delta_2{}^1(t)} &= M_2{}^{-1}\left(K_{s21}\frac{\Delta\delta_1{}^1(t)}{\Delta\delta_2{}^1(t)} - K_{s22} + +K_{s23}\frac{\Delta\delta_3{}^1(t)}{\Delta\delta_2{}^1(t)}\right) \\
\frac{\Delta\dot{\omega}_3^1(t)}{\Delta\delta_3{}^1(t)} &= M_3{}^{-1}\left(K_{s31}\frac{\Delta\delta_1{}^1(t)}{\Delta\delta_3{}^1(t)} + K_{s32}\frac{\Delta\delta_2{}^1(t)}{\Delta\delta_3{}^1(t)} - K_{s33}\right)
\end{aligned} \tag{15}$$

For mode 2:

$$\begin{aligned}
\frac{\Delta\dot{\omega}_1^2(t)}{\Delta\delta_1{}^2(t)} &= M_1{}^{-1}\left(-K_{s11} + K_{s12}\frac{\Delta\delta_2{}^2(t)}{\Delta\delta_1{}^2(t)} + K_{s13}\frac{\Delta\delta_3{}^2(t)}{\Delta\delta_1{}^2(t)}\right) \\
\frac{\Delta\dot{\omega}_2^2(t)}{\Delta\delta_2{}^2(t)} &= M_2{}^{-1}\left(K_{s21}\frac{\Delta\delta_1{}^2(t)}{\Delta\delta_2{}^2(t)} - K_{s22} + +K_{s23}\frac{\Delta\delta_3{}^2(t)}{\Delta\delta_2{}^2(t)}\right) \\
\frac{\Delta\dot{\omega}_3^2(t)}{\Delta\delta_3{}^2(t)} &= M_3{}^{-1}\left(K_{s31}\frac{\Delta\delta_1{}^2(t)}{\Delta\delta_3{}^2(t)} + K_{s32}\frac{\Delta\delta_2{}^2(t)}{\Delta\delta_3{}^2(t)} - K_{s33}\right)
\end{aligned} \tag{16}$$

Remarks

- Equations (15) and (16) provide the proposed transient stability margin of generators 1, 2, and 3 separately for modes 1 and 2, respectively.
- The proposed transient stability index considers the synchronizing torque contributions from other connected generators through the eigenvector information of each generator's rotor angle dynamic states of each electromechanical oscillation mode.

Results and Discussions

Note

- The proposed transient stability index is verified and compared on two test case simulations; a small WSCC 9-bus test system with three synchronous generators, and a large New England 68-bus test system with 16 synchronous generators (SGs) without considering exciter and governor dynamics.
- The MATLAB/Simulink-based open-source power system analysis toolbox (*PSAT*) is used for the simulations, and comparative studies.
- For the *t-d* simulations, the generators in the two test systems are modeled in subtransient machine models with negligible damping torque, and the loads are modeled with constant impedance models.

The simulations and analysis are performed over a range of critical operating points obtained by a slowly varying load factor λ. The λ vary the loads' active power demands according to Equation (17) as follows

$$P_L = P_{L0}\,(1 + \lambda) \tag{17}$$

where P_{L0} is the initial real power levels of the loads on the test systems.

Results and Discussions: The WSCC 9-Bus Test System

Table 1: Initial load bus data of the WSCC 9-bus test system for the simulations

Load Bus Name	Active Power Demand (pu) P_{L0}	Reactive Power Demand (pu) Q_{L0}
Load 5	1.25	0.5
Load 6	0.9	0.3
Load 8	1	0.35
Total	3.15	1.15

- The *WSCC* 9-bus test system's eigenvalue analysis resulted in two electromechanical oscillation modes due to the three generator interactions.
- The system's eigenvalues remained in the negative half of the s-plane, indicating a stable region of operating points over the range of λ values are considered for the simulations.
- The proposed transient stability index in Equation (13) and the detailed expressions in Equations (15) and (16) for each modes are utilized to determine generators' transient stability.

8

[8]: Data from the publicly available web page is used for the test cases https://icseg.iti.illinois.edu/power-cases/

Results and Discussions: The WSCC 9-Bus Test System

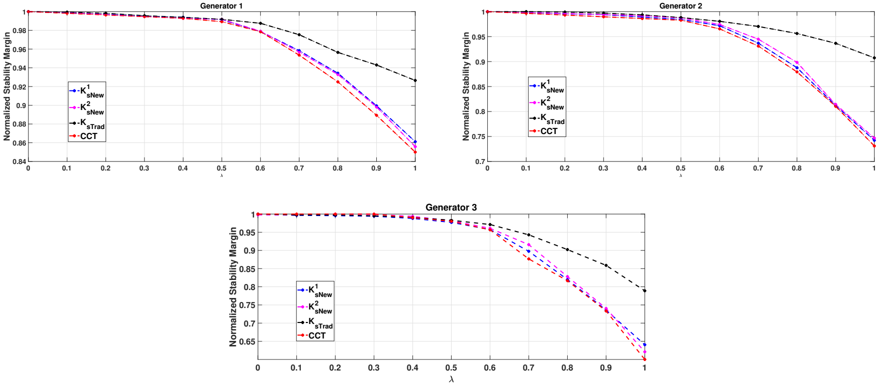

Figure 6: Transient stability margin of generators in WSCC 9-bus test system for mode 1 and mode 2.

Results and Discussions: The WSCC 9-Bus Test System

Remarks of Figure 6

- Figure 6 presents the variation of transient stability margins for generators 1, 2, and 3 as a function of λ, based on Equation (17), across the range from 0 to 1.
- The curves for K_{sTrad}, K^1_{sNew},K^2_{sNew}, and the CCT of all three generators exhibit a decreasing trend as λ increases, reflecting a corresponding decline in the system's overall transient stability. This observation supports the effectiveness of the proposed transient stability index.
- In all three generators, the proposed stability margin curves K^1_{sNew} and K^2_{sNew} closely follow the CCT curve and exhibit a trend that aligns more consistently compared to the traditional stability index, K_{sTrad}. This indicates that the proposed stability index offers a more accurate representation of transient stability and performs better.
- The normalized values of the stability margin's drop indicate that generator 3 suffers the most tremendous loss of stability, followed by generator 2, while generator 1 exhibits the best stability retention. This ranking of stability loss further corroborates the findings from the proposed index.

Results and Discussions: The New England 68-Bus Test System

Table 2: Initial load bus data of the New England 68-bus test system for the simulations

Load Bus Name	Active Power Demand (pu) P_{L0}	Reactive Power Demand (pu) Q_{L0}	Load Bus Name	Active Power Demand (pu) P_{L0}	Reactive Power Demand (pu) Q_{L0}
17	60	3	45	2.08	0.21
18	24.7	1.23	46	1.507	0.285
20	6.8	1.03	47	2.031	0.3259
21	2.74	1.15	48	2.412	0.022
23	2.48	0.85	49	1.64	0.29
24	3.09	-0.92	50	1	-1.47
25	2.24	0.47	51	3.37	-1.22
26	1.39	0.17	52	1.58	0.3
27	2.81	0.76	53	2.527	1.186
28	2.06	0.28	55	3.22	0.02
29	2.84	0.27	56	2	0.736
33	1.12	0	59	2.34	0.84
36	1.02	-0.1946	60	2.088	0.708
39	2.67	0.126	61	1.04	1.25
40	0.6563	0.2353	64	0.09	0.88
41	10	2.5	67	3.2	1.53
42	11.5	2.5	68	3.29	0.32
44	2.675	0.0484			
	continue		Total	176.2063	19.718

[9]

[9]: Data from the publicly available web page is used for the test cases https://icseg.iti.illinois.edu/power-cases/

Results and Discussions: The New England 68-Bus Test System

NOTE

- The New England 68-bus test system's eigenvalue analysis resulted in 15 electromechanical oscillation modes due to the 16 generator interactions.
- The system's eigenvalues remained in the negative half of the s-plane, indicating a stable region of operating points over the range of λ values are considered for the simulations.
- According to the proposed transient stability index, the transient stability margin of 16 generators for all 15 electromechanical modes can be determined.
- Based on a *t-d* stability indicator CCT of generators in the New England 68-bus test system, four generators—G_{13}, G_{14}, G_{15}, and G_{16}—were identified as critical due to their least and decreasing CCT values over a range of λ variations, as depicted in Figure 7.
- These generators exhibit the lowest transient stability margins compared to others and are the first to become unstable during disturbances.
- To gain deeper insights into the transient stability behavior, a focused analysis of these generators is conducted.

Results and Discussions: The New England 68-Bus Test System

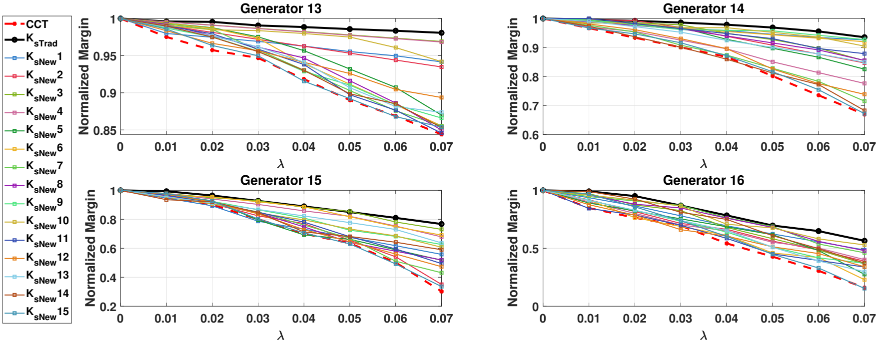

Figure 7: Transient stability analysis of generators 13 to 16 in New England 68-bus test system.

Results and Discussions: The New England 68-Bus Test System

Remarks of Figure 7

- It is evident that the proposed stability index, K^{h}_{sNew} for all the 15 modes, demonstrates superior performance compared to the traditional stability index, K_{sTrad}, for all generators by closely aligning with the CCT curves.
- However, including a larger number of modes complicates the overall stability analysis.
- The system's participation factor, derived from eigenvalue analysis, is used to filter the relevant modes corresponding to these critical generators, as shown in Figure 8.

Results and Discussions: The New England 68-Bus Test System

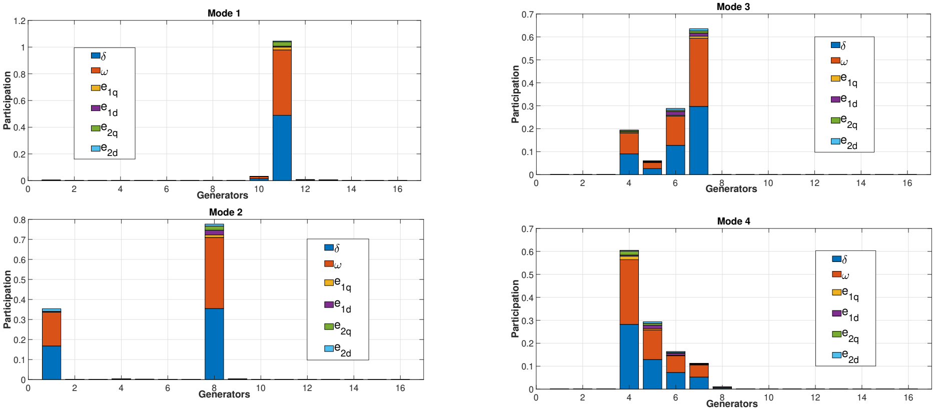

Figure 8: *Cont.*

- The X-axis of each graph indicates the generator number, and the Y-axis represents the stacked participation value of the corresponding generator's state variables δ, ω, e_{1q}, e_{1d}, e_{2q} and e_{2d} for subtransient machine models.

Results and Discussions: The New England 68-Bus Test System

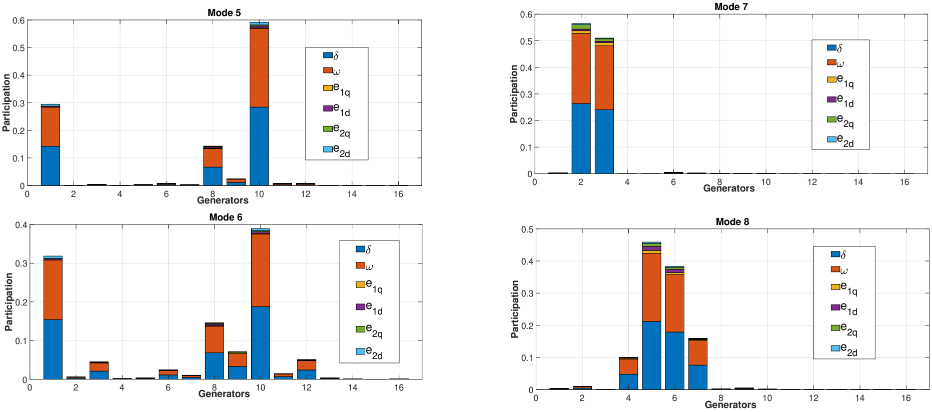

Figure 8: *Cont.*

Results and Discussions: The New England 68-Bus Test System

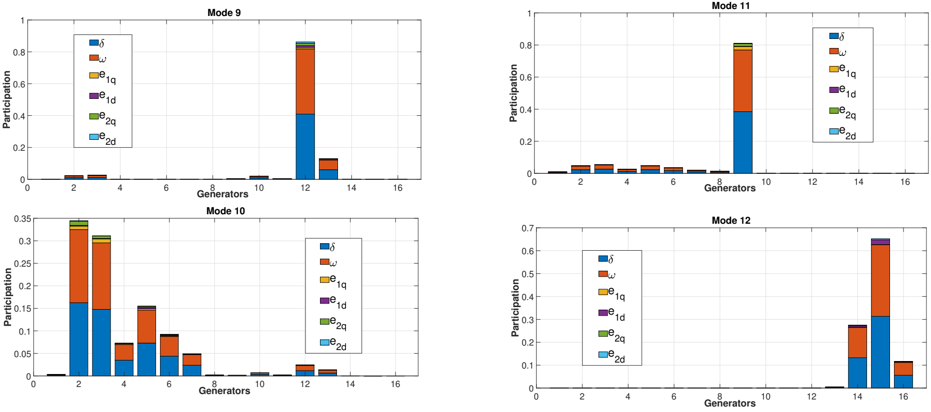

Figure 8: *Cont.*

Results and Discussions: The New England 68-Bus Test System

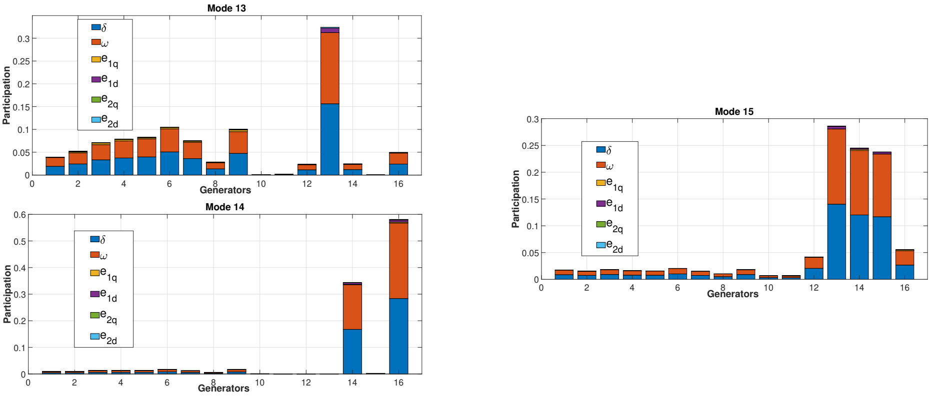

Figure 8: Participation factor information of electromechanical modes in New England 68-bus test system.

Results and Discussions: The New England 68-Bus Test System

Remarks of Figure 8

- The generators with δ and ω stacked participation greater than an assumed threshold value of 0.025 are considered the generators' valuable participation in the specified electromechanical modes, making more reliable stability remarks.
- Therefore critical generators with the most significant electromechanical modes can be summarized and shown in Table 3.
- Then the Figure 7 can be refined by focusing on the significant modes associated with these critical generators, as presented in Figure 9, to simplify the proposed *TSA* approach and provide more precise insights into the system's behavior.

Table 3: Critical generators with the most significant electromechanical modes.

Generators	**Most Significant Electromechanical Modes**
G_{13}	Mode 9, Mode 13, Mode 15
G_{14}	Mode 12,Mode 14, Mode 15
G_{15}	Mode 12, Mode 15
G_{16}	Mode 12, Mode 13, Mode 14, Mode 15

Results and Discussions: The New England 68-Bus Test System

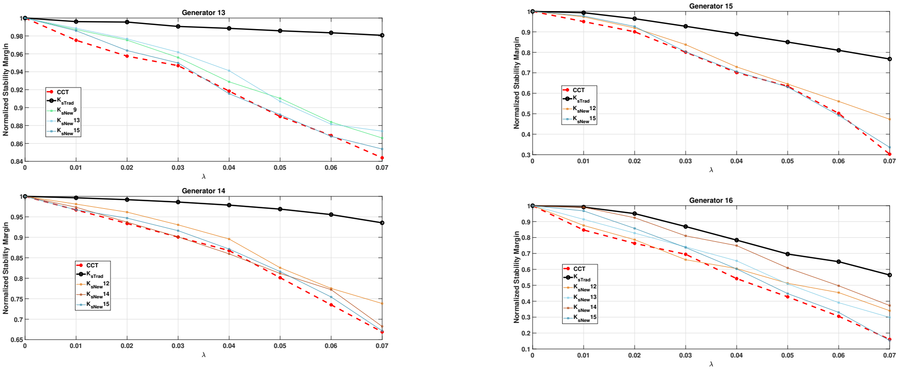

Figure 9: Transient stability analysis of critical generators in New England 68-bus test system.

Results and Discussions: The New England 68-Bus Test System

Remarks of Figure 9: Critical Generators with significant modes

- The stability margin curves derived from Figure 9 indicate that the proposed stability margin, based on the most associated modes of each generator, outperforms the traditional stability margin indicator, K_{sTrad}, in terms of stability performance.
- Additionally, the normalized stability margin reductions indicate that generator 16 exhibits the most significant loss of stability, closely followed by generator 15.
- In contrast, generators 13 and 14 demonstrate markedly better stability retention. This hierarchy of stability degradation aligns with the outcomes predicted by the proposed index, further substantiating its efficacy in accurately assessing system stability dynamics.

Overview

Related Journal Publication

- Poulose, Albert, and Soobae Kim. "Transient stability analysis and enhancement techniques of renewable-rich power grids." *Energies* 16.5 (2023): 2495.
- Poulose, Albert, and Soobae Kim. "Direct Transient Stability Assessment of Grid-Connected Voltage Source Converters: A Transient Energy Functions Perspective." *IEEE Access* , vol. 12, pp. 133545-133556, 2024

Direct Method of TSA

NOTE

- Determine stability without explicitly solving the system's differential equations.
- In many physical systems, Lyapunov functions have an energy function interpretation, which is the case with the power system model (Transient Energy Functions).

Lyapunov Functions

Consider a nonlinear autonomous and time-invariant dynamical system

$$\dot{x} = f(x)$$

where x is the state vector of dimension n, and the n-dimensional column vector f represents the nonlinear dynamics without external inputs and is not dependent on t. Let x_{ep} be an equilibrium point, that is $f(x_{ep}) = 0$.

Lyapunov Theorem: Let $V(x)$ be a positive definite scalar function of x (that is, $V(x) > 0$) in the neighborhood D of x_{ep} and $V(x_{ep}) = 0$. If

$$\dot{V}(x) = \frac{\partial V}{\partial x}\frac{dx}{dt} = \frac{dV}{dx}f(x) < 0$$

where the derivative $\frac{dV}{dx}$ is a row vector, for all $x \in D$ - $\{x_{ep}\}$, then x_{ep} is an asymptotically stable equilibrium, that is, $x \longrightarrow x_{ep}$ as $t \longrightarrow \infty$.

10

[10] Chow, Joe H., and Juan J. Sanchez-Gasca. Power system modeling, computation, and control. John Wiley & Sons, 2020.

Direct Method of TSA

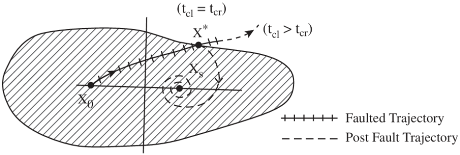

Figure 10: Region of attraction and computation of *CCT*.

11

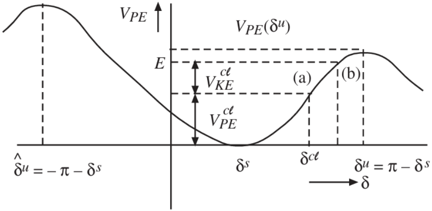

Figure 11: Potential Energy well.

---

[11] Sauer, Peter W., Mangalore A. Pai, and Joe H. Chow. Power system dynamics and stability: with synchrophasor measurement and power system toolbox. John Wiley & Sons, 2017.

Energy function for SMIB Electromechanical Model

Swing Equation:

$$\Delta\dot{\delta} = \Omega\Delta\omega$$
$$2H\dot{\Delta\omega} = P_m - \frac{EV}{X_{eq}}\sin\delta - D\Delta\omega \tag{18}$$

where E is the machine internal voltage, V is the voltage at the infinite bus, X_{eq} is the total reactance between the machine internal node and the infinite bus, and D represents the machine damping.

At the equilibrium point:

$$\omega = 0$$
$$\delta = \delta_{ep} = \sin^{-1}\frac{P_m X_{eq}}{EV} \tag{19}$$

If, $(\delta_{ep}, 0)$ is considered as stable equilibrium point $(\delta_{sep}, 0)$. Then the restoring torque about the equilibrium is

$$T_r = \frac{EV}{X_{eq}}\sin\delta - P_m \tag{20}$$

Therefore, potential energy

$$V_{PE}(\delta) = \int_{\delta_{sep}}^{\delta}\left(-P_m + \frac{EV}{X_{eq}}\sin\phi\right)d\phi \tag{21}$$

Note: The mathematical rule applied here is the dummy variable (ϕ) substitution in integration. The variable ϕ is used to ensure clarity and avoid confusion, while the integration limits δ_{sep} and δ define the range over which the function is integrated. The result is a function of δ, independent of the specific choice of the dummy variable.

Energy function for SMIB Electromechanical Model

Integrating (21)

$$V_{PE}(\delta) = -P_m\left(\delta - \delta_{sep}\right) - \frac{EV}{X_{eq}}\cos\delta + \frac{EV}{X_{eq}}\cos\delta_{sep} \tag{22}$$

Note: $V_{PE}(\delta_{sep}) = 0$ and $V_{PE}(\delta) > 0$ about $\delta = \delta_{sep}$.

Defining Kinetic energy of the rotating inertia as

$$V_{KE}(\omega) = \frac{1}{2}(2H)\omega^2 = H\omega^2 \tag{23}$$

Total transient energy is then

$$V_E(\delta, \omega) = V_{PE}(\delta) + V_{KE}(\omega) > 0 \tag{24}$$

Therefore,

$$\begin{aligned}
\dot{V}_E &= \frac{dV_E}{dt} \\
&= \frac{dV_{PE(\delta)}}{d\delta}\frac{d\delta}{dt} + \frac{dV_{KE}(\omega)}{d\omega}\frac{d\omega}{dt} \\
&= \left(-P_m + \frac{EV}{X_{eq}}\sin\delta\right)\omega + 2H\omega\frac{d\omega}{dt} \\
&= \omega\left(2H\frac{d\omega}{dt} - P_m + \frac{EV}{X_{eq}}\sin\delta\right) \\
&= -D\omega^2 < 0
\end{aligned} \tag{25}$$

Thus, from the Lyapunov Theorem, the equilibrium point $(\delta_{sep}, 0)$ is asymptotically stable.

System Description

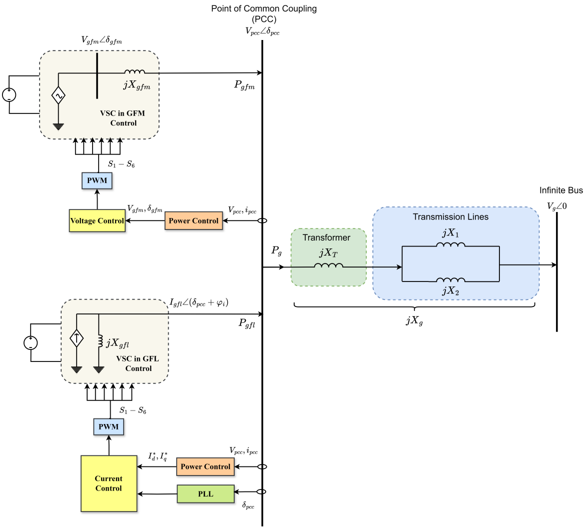

Figure 12: Single-line diagram of the GFL-VSC and GFM-VSC interconnected RES system.

System Description

- The modelling of *RES* connection to the *PCC* through a *VSC* interface, employing *GFL* with standard *PLL*- assisted vector current control and a *GFM* with *VSM* control strategies and an infinite bus is established with transformer (X_T) and a parallel transmission line (X_g) as depicted in Figure 12.
- The power controller in *GFL-VSC* establishes the current references throughout the converter's regular operation. However, in the event of faults, it supplies reactive current that depends on voltage according to the grid code while allowing for flexibility in the active current reference to ensure an active power supply.
- Therefore, the reference value of the *GFL-VSC* is adjusted according to different grid operating conditions, leading to corresponding changes in the magnitude of the current and the power factor angle.
- For ease of representation, the transient reactance of the *VSC* and transformer reactances of the converter configurations are inherited into the internal reactance of X_{gfl} in parallel with the equivalent current source model of *GFL*, and a series reactance of X_{gfm} internal to an equivalent voltage source model of *GFM*.
- In this study, the electromechanical virtual rotor transient dynamics of *GFM-VSC* are focused, and all other electromagnetic transients, including lines, are disregarded. Thus, phasor models of *GFL-VSC* and lines are adopted to characterize their influence on electro-mechanical transient instability without considering the current limiting characteristic of converters.
- Specifically, considering that the *GFL-VSC* operates at full power and enters saturation mode during faults due to voltage sag, it is assumed to act as a current source with magnitude I_{gfl} and phase $\delta_{pcc+\varphi_i}$, contributing to the power flow P_{gfl} to the *PCC*.
- Furthermore, V_{gfm} and δ_{gfm} denote the magnitude and phase angle of the equivalent voltage source of *GFM-VSC*, respectively, with corresponding power flow P_{gfm} into the *PCC*. The *PCC*'s voltage magnitude and phase angles are represented by V_{pcc} and δ_{pcc}, respectively, with power P_g injected into the grid without considering any losses in the network.

System Description

By applying the superposition principle to Figure 12, the voltage equations in the synchronous reference frame can be formulated as follows:

$$V_{pcc}e^{0} = a_1 V_{gfm} e^{j(\delta_{gfm} - \delta_{pcc})} + a_2 V_g e^{-j\delta_{pcc}} + ja_3 I_{gfl} e^{\varphi_i} \tag{26}$$

where

$$X_g = X_T + \frac{X_1 X_2}{X_1 + X_2}, a_1 = \frac{X_g}{X_g + X_{gfm}}, a_2 = \frac{X_{gfm}}{X_g + X_{gfm}}, a_3 = \frac{X_g X_{gfm}}{X_g + X_{gfm}}$$

Thus, the magnitude of the voltage at the *PCC* can be determined from Equation (26).

$$|V_{pcc}| = \sqrt{\frac{G + \sqrt{G^2 - 4a_3^2 P_{gfl}^2}}{2}} \tag{27}$$

where

$$G = a_1^2 V_{gfm}^2 + 2a_1 a_2 V_g V_{gfm} cos\delta_{gfm} + a_2^2 V_g^2$$

Additionally, the relationship between δ_{gfm} and δ_{pcc} can be derived from Equation (26) as follows:

$$\delta_{pcc} = sin^{-1}\left(\frac{a_1 a_2 P_{gfl} V_{gfm}}{GV_{pcc}} cos\delta_{gfm} + \frac{a_2 a_3 P_{gfl} V_g}{GV_{pcc}} + \frac{a_1 V_{gfm} V_{pcc}}{G} sin\delta_{gfm}\right) \tag{28}$$

[12] [13]

[12] He, Xiuqiang, and Hua Geng. "Transient stability of power systems integrated with inverter-based generation." IEEE Transactions on power systems 36.1 (2020): 553-556.

[13] Liu, Xinyu, et al. "Transient stability of synchronous condenser co-located with renewable power plants." IEEE Transactions on Power Systems 39.1 (2023): 2030-2041.

Transient Stability Mechanism

- Transient stability in power systems is evaluated by simulating fault conditions on various system elements and analyzing their impact on dynamic state variables.
- The simulation process comprises pre-fault, fault-on, and post-fault periods.
- These dynamic simulations aim to determine whether the power system stabilizes and converges to a new equilibrium state post-fault.

Pre-fault period

Represents the steady-state power flow condition, where initial parameters are set to balance power supply and load demand.

Fault-on period

Begins when a fault occurs and persists until it is cleared by circuit breaker action, during which the generator rotor accelerates due to the disturbance in electrical power transfer.

Post-fault period

The system enters this period upon clearing the fault, typically resulting in a weakened system state (Here, the post-fault system is assumed to be the same as the pre-fault by considering self-clearing fault).

Transient Stability Mechanism: Pre-fault Period

GFL-VSC

- During the pre-fault period or steady-state operation, the *GFL-VSC* with standard *PLL*-assisted vector current control acts as a current source that follows the grid, supplying power P_{gfl} with a current I_{gfl}.
- Typically, *RES* connected in *GFL* connection strategies does not inherently generate reactive power during normal operation; hence, the *d-q* current components can be computed under the assumption of a unity power factor to inject maximum active power through the current component of the *GFL-VSC*.

$$I_{gfl_d} = \frac{P_{ref}}{V_{pcc}}$$

$$I_{gfl_q} = \frac{-Q_{ref}}{V_{pcc}}$$

where $P_{ref} = P^*_{gfl}$ and $Q_{ref} = 0\ p.u.$ to maintain unity power factor.

Transient Stability Mechanism: Pre-fault Period

GFM-VSC

The active power delivered by *GFM-VSC* to the grid can be derived as follows:

$$P_{gfm} = P_g - P_{gfl}$$
$$= \frac{|V_{pcc}||V_g|}{X_g} sin\delta_{pcc} - P_{gfl}$$
$$= \frac{a_1 a_2 P_{gfl} V_{gfm} V_g}{G} cos\delta_{gfm} + \frac{a_2 a_3 P_{gfl} V_g^2}{GXg} + \frac{a_1 V_{gfm} V_g \left(G + \sqrt{G^2 - 4a_3^2 {P_{gfl}}^2} \right)}{2GX_g} sin\delta_{gfm} - P_{gfl} \tag{29}$$

The virtual rotor swing equation of the $GFM - VSC$ with VSM within the associated system can be delineated analogously to the swing equation of SGs, as shown below.

$$\dot{\delta}_{gfm} = \Omega \Delta\omega_{gfm} \tag{30}$$

$$\dot{\Delta\omega}_{gfm} = \frac{1}{2H_{gfm}} \left(P^*_{gfm} - P_{gfm} - D_{gfm} \Delta\omega_{gfm} \right) \tag{31}$$

where $\Omega = 2\pi f$ is the per-unit to the radian conversion factor for speed change, P^*_{gfm} is the reference power setting on the *GFM-VSC*, $\Delta\omega_{gfm}$ represents the relative angular speed variations of the *GFM-VSC*, H_{gfm} denotes the virtual inertia contribution from the *GFM-VSC*, and D_{gfm} signifies the virtual damping coefficient contribution from the *GFM-VSC*.

Transient Stability Mechanism: Fault-on period

GFM-VSC

In the event of a three-phase short-circuit fault at the mid-point of one of the transmission lines, the voltage at the *PCC* decreases to $V_{pcc_{fault}}$, while the internal voltage of the *GFM-VSC*, V_{gfm}, is assumed to remain constant, as depicted in Figure 13.

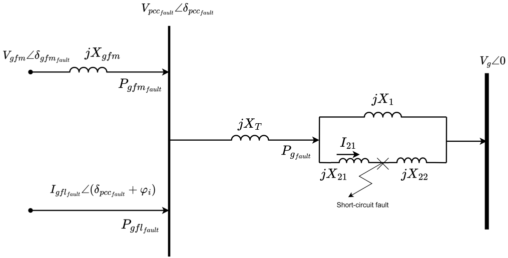

Figure 13: The equivalent circuit diagram of the *GFM-VSC* and *GFL-VSC* interconnected RES system shows a short-circuit fault on one of the parallel lines.

Transient Stability Mechanism: Fault-on period

- The electrical power output of the $GFM - VSC$ during the fault, represented as $P_{gfm_{fault}}$, is determined by constructing a Thevenin equivalent circuit using the high-side voltage of the transformer as the output port.

Thevenin equivalent circuit

- In this configuration, the voltage sources $V_{gfm}\angle\delta_{gfm_{fault}}$ and $V_g\angle 0$ are combined into a single equivalent voltage source, while the reactances of the transmission line and transformer are consolidated into one series reactance.
- Notably, the reactance jX_{22} is excluded from this calculation.
- Following this, the open-circuit voltage V_{oc} and the short-circuit current I_{21} in the transmission line with impedance jX_{21} are determined by analyzing the open-circuit and short-circuit conditions separately.

Transient Stability Mechanism: Fault-on period

Open-circuit condition

The open-circuit condition is imposed on the system, and the revised representation of the system is depicted in Figure 14

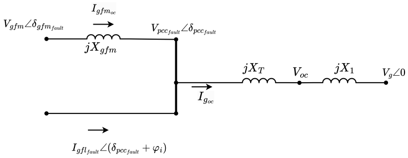

Figure 14: Open circuit representation of the system.

$$I_{g_{oc}} = I_{gfm_{oc}} + I_{gfl_{fault}} \tag{32}$$

$$I_{g_{oc}} = \frac{V_{pcc_{fault}}\angle\delta_{pcc_{fault}} - V_g\angle 0}{jX_T + jX_1} \tag{33}$$

$$I_{gfm_{oc}} = \frac{V_{gfm}\angle\delta_{gfm_{fault}} - V_{pcc_{fault}}\angle\delta_{pcc_{fault}}}{jX_{gfm}} \tag{34}$$

Therefore,

$$V_{oc} = V_{gfm}\angle\delta_{gfm_{fault}} - I_{gfm_{oc}} jX_{gfm} - I_{g_{oc}} jX_T \tag{35}$$

Transient Stability Mechanism: Fault-on period

Short-circuit condition

The short-circuit condition is applied to the system, and the updated depiction of the system is illustrated in Figure 15

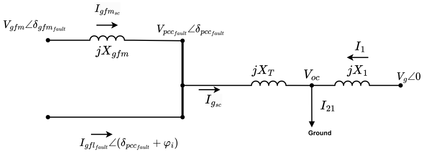

Figure 15: Short circuit representation of the system.

$$I_{gfm_{sc}} = \frac{V_{gfm}\angle\delta_{gfm_{fault}} - V_{pcc_{fault}}\angle\delta_{pcc_{fault}}}{jX_{gfm}} \quad (36)$$

$$I_{g_{sc}} = I_{gfm_{sc}} + I_{gfl_{fault}} \quad (37)$$

$$\begin{aligned} I_{21} &= I_1 + I_{gsc} \\ &= \frac{V_g\angle 0}{jX_1} + I_{gsc} \end{aligned} \quad (38)$$

Transient Stability Mechanism: Fault-on period

Thevenin equivalent circuit

Accordingly, the Thevenin equivalent circuit can be formed using the open-circuit voltage and short-circuit current equations, as illustrated in Figure 16.

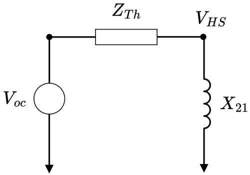

Figure 16: Thevenin equivalent circuit representation of the system

The equations for the equivalent Thevenin impedance and voltage are provided below:

$$
\begin{aligned}
Z_{Th} &= \frac{V_{oc}}{I_{21}} \\
V_{HS} &= \frac{jX_{21}}{Z_{Th} + jX_{21}} V_{oc}
\end{aligned}
\tag{39}
$$

Transient Stability Mechanism: Fault-on period

GFM-VSC

The Thevenin equivalent voltage V_{HS} is a function of δ and thus varies with time.

$$I_{g_{fault}} = \frac{V_{pcc_{fault}} \angle \delta_{pcc_{fault}} - V_{HS}}{jX_T} \quad (40)$$

$$I_{gfm_{fault}} = I_{g_{fault}} - I_{gfl_{fault}} \quad (41)$$

$$P_{gfm_{fault}} = Re\left[\left(V_{gfm} \angle \delta_{gfm_{fault}}\right) I_{gfm_{fault}}\right] \quad (42)$$

GFL-VSC

- On the other side, the *GFL-VSC* adopts low voltage ride through (*LVRT*) mode as its control scheme in accordance with the grid code during fault time.
- The *d-q* currents from the *GFL-VSC* are promptly modified using pre-defined algorithms.

$$\begin{aligned} I_{gfl_{q_{fault}}} &= I_{gfl_0} + K(0.9 - V_{pcc}),\, V_{pcc} < 0.9p.u \\ I_{gfl_{fault}} = I_{gfl_{d_{fault}}} &= \sqrt{I_{max}^2 - I_{gfl_{q_{fault}}}^2} \end{aligned} \quad (43)$$

where I_{gfl_0} is the device's prefault current. I_{max} is the value of saturation current. K is the Q-V_{pcc} gain coefficient

Proposed DTSA Methodology

Energy Functions for GFM-VSC associated System

- At the equilibrium point, the state variables of the *GFM-VSC*, $(\delta_{gfm}, \Delta\omega_{gfm})$, transition to $\left(\delta_{gfm_{ep}}, 0\right)$, and P_{gfm} equals P^*_{gfm} as derived from Equation (31).
- Hence, the revised form of Equation (29) is as follows:

$$\begin{aligned} P^*_{gfm} &= P_g - P_{gfl} \\ &= \frac{a_1 a_2 P_{gfl} V_{gfm} V_g}{G_{ep}} cos\delta_{gfm_{ep}} + \frac{a_2 a_3 P_{gfl} V_g^2}{G_{ep} Xg} \\ &+ \frac{a_1 V_{gfm} V_g \left(G_{ep} + \sqrt{G_{ep}^2 - 4a_3^2 {P_{gfl}}^2}\right)}{2G_{ep}X_g} sin\delta_{gfm_{ep}} - P_{gfl} \end{aligned} \tag{44}$$

where

$$G_{ep} = a_1^2 V_{gfm}^2 + 2a_1 a_2 V_g V_{gfm} cos\delta_{gfm_{ep}} + a_2^2 V_g^2$$

The restoring torque about the equilibrium point is

$$T_r = P_{gfm} - P^*_{gfm} \tag{45}$$

The kinetic energy generated by the virtual inertia on the *GFM-VSC* is expressed as

$$V_{KE}\left(\Delta\omega_{gfm}\right) = \frac{1}{2}\left(2H_{gfm}\right)\Delta\omega^2_{gfm} \tag{46}$$

Proposed DTSA Methodology

Energy Functions for GFM-VSC associated System

- Furthermore, the equilibrium point, denoted by $\left(\delta_{gfm_{ep}}, 0\right)$, is assumed to be the stable equilibrium point $\left(\delta_{gfm_{sep}}, 0\right)$.
- Consequently, the potential energy can be expressed as the integral of the restoring torque developed across the *GFM-VSC*, as detailed in Equation (47).

$$
\begin{aligned}
V_{PE}\left(\delta_{gfm}\right) &= \int_{\delta_{gfm_{sep}}}^{\delta_{gfm}} \left(P_g - P_{gfl} - P_{gfm}^{*}\right) d\phi \\
&= -P_{gfl}\left(\delta_{gfm} - \delta_{gfm_{sep}}\right) - P_{gfm}^{*}\left(\delta_{gfm} - \delta_{gfm_{sep}}\right) + \int_{\delta_{gfm_{sep}}}^{\delta_{gfm}} P_g \, d\phi
\end{aligned}
\tag{47}
$$

where

$$
\int_{\delta_{gfm_{sep}}}^{\delta_{gfm}} P_g \, d\phi = \int_{\delta_{gfm_{sep}}}^{\delta_{gfm}} \left(\frac{a_1 a_2 P_{gfl} V_{gfm} V_g}{G_{sep}} cos\phi + \frac{a_2 a_3 P_{gfl} V_g^2}{G_{sep} X_g} + \frac{a_1 V_{gfm} V_g \left(G_{sep} + \sqrt{G_{sep}^2 - 4a_3^2 {P_{gfl}}^2}\right)}{2 G_{sep} X_g} sin\phi \right) d\phi
$$

Proposed DTSA Methodology

Energy Functions for GFM-VSC associated System

Consequently, the total transient energy is

$$V_E(\delta_{gfm}, \Delta\omega_{gfm}) = V_{PE}(\delta_{gfm}) + V_{KE}(\Delta\omega_{gfm}) > 0 \tag{48}$$

Taking time derivative of the Equation (48)

$$\begin{aligned} \dot{V}_E &= \frac{dV_E}{dt} \\ &= \frac{dV_{PE}(\delta_{gfm})}{d\delta_{gfm}}\frac{d\delta_{gfm}}{dt} + \frac{dV_{KE}(\Delta\omega_{gfm})}{d\Delta\omega_{gfm}}\frac{d\Delta\omega_{gfm}}{dt} \end{aligned} \tag{49}$$

where

$$\begin{aligned} \frac{dV_{PE}(\delta_{gfm})}{d\delta_{gfm}} &= -P_{gfl} - P^*_{gfm} + \frac{a_2 a_3 P_{gfl} V_g^2}{G} + \frac{a_1 a_2 P_{gfl} V_{gfm} V_g \cos\delta_{gfm}}{G} \\ &- \frac{a_1 V_{gfm} V_g \left(G + \sqrt{G^2 - 4a_3^2 {P_{gfl}}^2}\right)\sin\delta_{gfm}}{2GX_g} \end{aligned} \tag{50}$$

and

$$\frac{dV_{KE}(\Delta\omega)}{d\Delta\omega} = 2H_{gfm}\Delta\omega_{gfm} \tag{51}$$

Proposed DTSA Methodology

Energy Functions for GFM-VSC associated System

Upon substitution of Equation (50) and Equation (51) into Equation (49), the expression governing the rate of change of V_E, denoted by Equation (52), is derived.

$$\begin{aligned}\dot{V_E} &= \left(-P_{gfl} - P^*_{gfm} + \frac{a_2^2 P_{gfl} V_g^2}{G} + \frac{a_1 a_2 P_{gfl} V_{gfm} V_g \cos\delta_{gfm}}{G} - \frac{a_1 V_{gfm} V_g \left(G + \sqrt{G^2 - 4a_3^2 P_{gfl}^2}\right)\sin\delta_{gfm}}{2GX_g}\right)\Delta\omega_{gfm} \\ &+ \left(2H_{gfm}\Delta\omega_{gfm}\right)\frac{d\Delta\omega_{gfm}}{dt} \\ &= \Delta\omega_{gfm}\left(-P_{gfl} - P^*_{gfm} + \frac{a_2^2 P_{gfl} V_g^2}{G} + \frac{a_1 a_2 P_{gfl} V_{gfm} V_g \cos\delta_{gfm}}{G} - \frac{a_1 V_{gfm} V_g \left(G + \sqrt{G^2 - 4a_3^2 P_{gfl}{}^2}\right)\sin\delta_{gfm}}{2GX_g} + 2H_{gfm}\frac{d\Delta\omega_{gfm}}{dt}\right)\end{aligned} \tag{52}$$

Proposed DTSA Methodology

Energy Functions for GFM-VSC associated System

Moreover, by utilizing Equation (29) and Equation (31), Equation (52) is further transformed into Equation (53)

$$\begin{aligned}\dot{V}_E &= \Delta\omega_{gfm}\left(-P^*_{gfm} + P_{gfm} + 2H_{gfm}\frac{d\Delta\omega_{gfm}}{dt}\right)\\ &= -D_{gfm}\Delta\omega^2_{gfm} < 0\end{aligned} \tag{53}$$

Thus, according to the Lyapunov Theorem, the assumed point $\left(\delta_{gfm_{sep}}, 0\right)$ is asymptotically stable.

Proposed DTSA Methodology

DTSA criterion

- In conservative systems, the total transient energy V_E at the stability limit is termed as V_{crit}, which also corresponds to the potential energy at the unstable equilibrium point $\left(\delta_{gfm_{uep}}, 0\right)$.

$$V_{crit} = V_{PE}\left(\delta_{gfm_{uep}}\right) \tag{54}$$

  where $\delta_{gfm_{uep}} = 180 - \delta_{gfm_{ep}}$ for a grid connected system with single $GFM - VSC$.
- If the accumulated $V_E > V_{crit}$ at the fault clearing time, then the system is unstable, and if the fault is cleared at $V_E(t_c) < V_{crit}$, then the system is stable.
- The corresponding value of the system's CCT, $t_c = t_{crit}$ is obtained at the point where the $V_E(t_{crit}) = V_{crit}$.
- The immediate benefit of this approach is eliminating the requirement to simulate the post-fault system, which typically requires an extended simulation duration to assess transient stability comprehensively.

Results and Discussions

- To evaluate the *TSA* of the interconnected system comprising the *GFM-VSC* and *GFL-VSC*, as illustrated in Figure 12, the proposed *DTSA* approach is implemented in the Matlab programming environment.
- The system parameters specified in Table 4 are utilized for this analysis.

Table 4: *Cont.*

Parameters	Value
Voltage base, V_{base}	400 kV
Power base, S_{base}	1000 MVA
Frequency base, f_0	60 Hz
Nominal dc voltage (Perfect DC source)	640 kV
Voltage of infinite AC bus, V_g	$1p.u.$
Short Circuit Ratio, *SCR*	2
Reactance of transmission line, $X_g = X_T + X_1 \|\| X_2$	0.1 $p.u.$ + 0.25 $p.u.$
Simulation time	10 s
Simulation time step	25 μs
GFM Parameters	
GFM active power set point, P_{gfm}	1000 MW
GFM voltage, V_{gfm}	1.03 $p.u.$
GFM internal series reactance, X_{gfm}	0.01 $p.u.$
Control strategy	*VSM*
Virtual inertia, H_{gfm}	5 s
Virtual damping ratio, D_{gfm}	1
Transient damping resistance, R_v	0.09 Ω
Current saturation limit	1.2 $p.u$
Bandwidth	300 rad/s

Table 4: Simulation Parameters of the System.

Parameters	Value
GFL Parameters	
GFL active power set point, P_{gfl}	1000 MW
GFL internal parallel reactance, X_{gfl}	10 $p.u.$
PLL bandwidth	60 rad/s
Damping ratio	1
Outer loop mode	Voltage Control
Power control bandwidth	6 rad/s
Voltage control bandwidth	10 rad/s
Low-pass filters bandwidth	30 rad/s
Current loop bandwidth	4000 rad/s

Results and Discussions

Proposed DTSA using Energy Function Plot

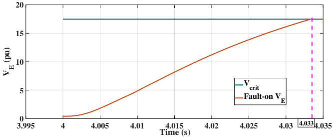

(A) Stable FCT of 33 ms

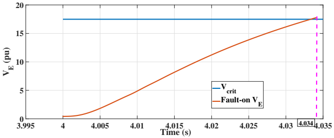

(B) Unstable FCT of 34 ms

Figure 17: Proposed DTSA

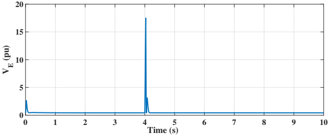

(A) Stable V_E variations over the simulation period of 10 s

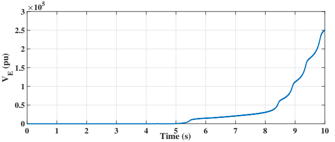

(B) Unstable V_E variations over the simulation period of 10 s

Figure 18: V_E variations over the simulation period of 10 s

Results and Discussions

Proposed DTSA using Energy Function Plot

- In the proposed *DTSA* method, the V_E (defined in (49)) and the V_{crit} (defined in (54)) are plotted in Figure 17a and Figure 17b.
- The intersection of the V_E and V_{crit} curves in both figures is pivotal for determining the system's *CCT*, which is found to be 33 ms for the system under study.
- A *CCT* of 33 ms indicates the system will become unstable if a fault persists beyond this threshold duration. Conversely, if the fault is cleared within 33 ms, V_E remains below V_{crit}, enabling system recovery and ensuring stable operation.
- This study presents two graphs: Figure 17a shows a stable case with a fault clearing time (*FCT*) of 33 ms, while Figure 17b illustrates an unstable case with an *FCT* of 34 ms.
- To further elucidate this concept, the variations in V_E over the simulation period for both stable and unstable cases are depicted in Figure 18a and Figure 18b.
- In the stable case, the minimal nominal energy level of *GFM-VSC*'s V_E experiences a pronounced spike during a disturbance at 4s.
- Following the fault-on period, which cleared at 4.033 s, V_E returns to its initial level, as illustrated in Figure 18a.
- This stable response is ensured as the V_E level remains below V_{crit} during the fault-on period with a fault duration of 33 ms.
- Conversely, Figure 18b illustrates the unstable response throughout the simulation period due to the surpasses level of V_E over V_{crit} during the fault-on period with a fault duration of 34 ms, leading to an uncontrolled increase in V_E over the simulation time, resulting in the instability of the *GFM-VSC*.

Results and Discussions

Time Domain Simulation Responses

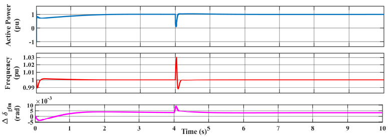

(A) For the FCT of 33ms

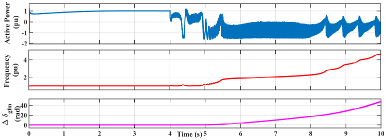

(B) For the FCT of 34ms

Figure 19: GFM-VSC t-d simulation response

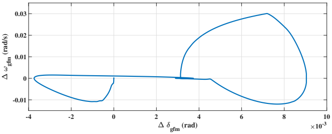

(A) For the FCT of 33ms

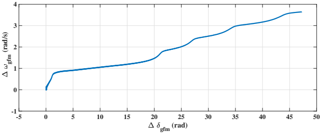

(B) For the FCT of 34ms

Figure 20: Phase portrait response of the GFM-VSC

Results and Discussions

Time Domain Simulation Responses

- In the proposed *DTSA* method, the V_E (defined in (48)) and the V_{crit} (defined in (54)) are plotted in Figure 17a with a fault clearing time (FCT) of 33 ms, while Figure 17b illustrates an unstable case with an FCT of 34 ms.
- The intersection of the V_E and V_{crit} curves in both figures is pivotal for determining the system's CCT, which is found to be 33 ms for the system under study.
- A CCT of 33 ms indicates the system will become unstable if a fault persists beyond this threshold duration. Conversely, if the fault is cleared within 33 ms, V_E remains below V_{crit}, enabling system recovery and ensuring stable operation.
- To further elucidate this concept, the variations in V_E over the simulation period for both stable and unstable cases are depicted in Figure 18a and Figure 18b.
- In the stable case, the minimal nominal energy level of *GFM-VSC*'s V_E experiences a pronounced spike during a disturbance at 4s. Following the fault-on period, which cleared at 4.033 s, V_E returns to its initial level, as illustrated in Figure 18a.
- This stable response is ensured as the V_E level remains below V_{crit} during the fault-on period with a fault duration of 33 ms.
- Conversely, Figure 18b illustrates the unstable response throughout the simulation period due to the surpasses level of V_E over V_{crit} during the fault-on period with a fault duration of 34 ms, leading to an uncontrolled increase in V_E over the simulation time, resulting in the instability of the *GFM-VSC*.

Overview

Contributions

1. Conventional Power System TSA

A model-based transient stability index for each generator is proposed from the synchronizing torque contributions of all other connected generators in a multi-machine interconnected power system.

- Power systems with more generators and electromechanical modes complicate the proposed *TSA* index.
- The decoupling nature of inverters limits the proposed approach on *RES* connected power systems.

2. Renewable Connected Power System TSA

Proposes an innovative fast direct transient stability analysis (*DTSA*) approach that leverages Lyapunov's direct method to assess the transient stability of a *GFM* with *VSM* control technique, incorporating the influence of parallel-connected *VSC* with *GFL* control strategy.

- This study focuses on systems featuring a single *VSC* under the *GFM* control strategy, which leads to a single unstable equilibrium point. Therefore, the computation of critical energy becomes relatively straightforward yet innovative in the context of this specific research domain.
- The proposed approach relies on obtaining internal reactance values of *VSCs* from manufacturers, which limits its broader applicability in practice.

Future Works

1. Adapt and apply advanced *TSA* techniques such as the potential energy boundary surface (*PEBS*) method, the controlling unstable equilibrium method, and the boundary-of-stability-region-based controlling unstable equilibrium point (*BCU*) methods to the systems comprising multiple $GFM - VSC$s.
2. The proposed *DTSA* approach, *VSC*s are assumed to operate without current limitations, and the equations are derived based on ideal sinusoidal P-δ curve characteristics. However, in practical applications, *VSC*s are subject to current constraints, leading to flat regions in the P-δ curves. Addressing these current-limited scenarios will be an additional focus of future work.
3. Determine the impact of reactive power sources such as synchronous condensers and FACT devices on the transient stability of VSCs
4. Apply Data-driven based methods utilizing machine learning and artificial intelligence techniques to accomplish *TSA*.

THANK YOU

Overview

Critical Clearing Time (CCT) and System Stability

The CCT is the maximum duration a power system can tolerate in the fault-on state without becoming unstable before removing the fault.

Remarks

- It should be noted that a CCT is specific to the fault's type and location applied to the system, and it is explicitly stated that the normal fault clearing time is often much shorter than the CCT values.
- The CCT is a valuable metric for power system design and operation studies because it allows comparison of the severity of different conditions and effectiveness of numerous interventions such as generation dispatches, control modifications, or network reinforcements.
- Thus, each generator's transient stability limit can be determined by applying a three-phase fault near the generators and measuring the CCT values by varying the fault duration on the system.

Important Power System Terms

Inertia

- Inertia in a power system refers to the resistance of the system to changes in its rotational speed (i.e., the speed at which generators rotate) due to disturbances. In other terms, it refers to the stored energy present in large rotating generators, which provides them with the ability to remain rotating and maintain speed when there are disruptions in the system.
- It provides the necessary time buffer during disturbances, ensuring the system stabilizes before severe issues.
- **Inertia constant:** Represents the amount of kinetic energy stored in the rotating mass of a generator's rotor at synchronous speed, normalized by the generator's rated power.

Eigen values

- Eigenvalues of the state matrix (information about the system's dynamics) provide information about the system's stability, which can be obtained from the system matrix.

Modes

- Modes refer to the natural oscillatory patterns that arise in a power system in response to disturbances.
- Each mode has a frequency and a damping ratio, which describe how fast it oscillates and how quickly the oscillation dies down. It is identified from the system's eigenvalues, where each eigenvalue corresponds to a specific mode of oscillation.
- **Electromechanical Modes:** These are low-frequency oscillations (typically 0.1 to 2 Hz) associated with the interactions between synchronous machines (State variables involved: δ and ω).

Important Power System Terms

Left Eigenvector

- Provide information about the sensitivity of the modes to external inputs (like disturbances or control actions)
- Determine how control inputs or disturbances affect each mode, which is crucial for designing effective control strategies to enhance stability.

Right Eigenvector/ Mode Shape

- Describe how the oscillation of a specific mode is distributed across different generators or system components.
- It helps to identify which parts of the system are oscillating in-phase or out-of-phase, providing insight into how the oscillation propagates through the network.
- This information is valuable for designing controllers or placing power system stabilizers to dampen specific modes and improve system stability.
- **Mode Shape:** Is the physical interpretation of the right eigenvector in the context of power system dynamics.

Participation Factor

- Offer deeper information by combining right and left eigenvectors (product is a scalar value) to determine how much each state variable contributes to and influences a particular mode.

Classification of Grid Connected Inverters

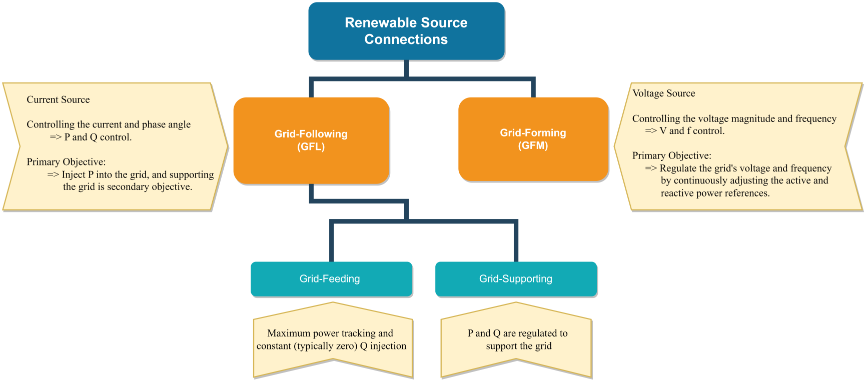

Figure 21: Distinguishing characteristics of *GFL* and *GFM*.

Voltage Source Converter (VSC) control structure

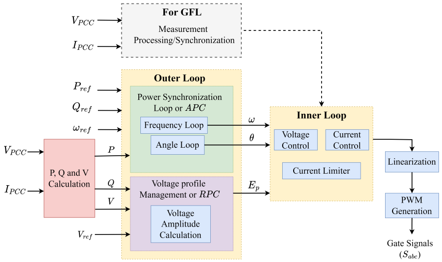

Figure 22: Generalized control structure of *VSC*.

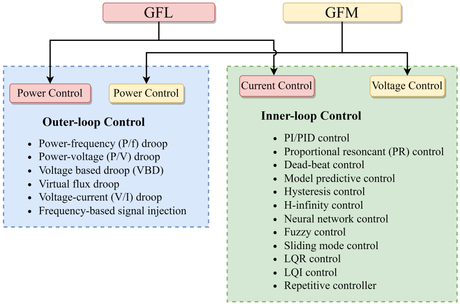

Figure 23: Control techniques for outer and inner control loops.

VSC with Virtual Inertia

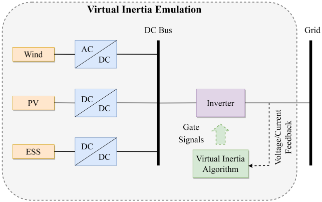

Figure 24: Concept of Virtual Inertia.

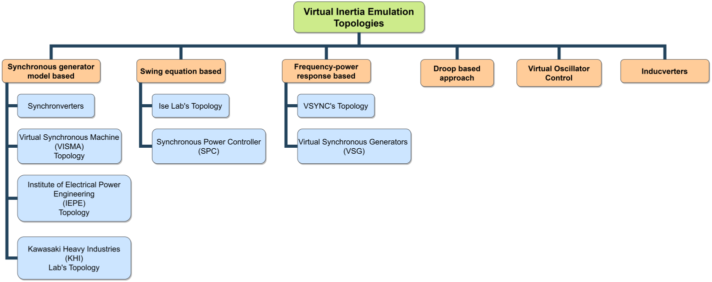

Figure 25: Virtual inertia implementation topologies.